



Synthesis, Characterization and DNA Binding Studies of (E)-1-((Pyridin-2-yl)methylidene) semicarbazide Mn(II), Co(II), Ni(II) and Cu(II) Complexes

**Oinam U-wang¹, R. K. Bhubon Singh^{1*}, W. Bembee Devi¹,
U. Ibotomba Singh¹, R. K. Bindiya Devi¹, O. Bijeta Devi¹, Ramina¹,
Th. Surchandra Singh¹ and Toka Swu²**

¹Department of Chemistry, Manipur University, Canchipur- 795003, Manipur, India.

²Department of Chemistry, Pondicherry University, R.V. Nagar, Kalapet, Puducherry 605014, India.

Authors' contributions

This work was carried out in collaboration among all authors. Author RKBS designed the study. Author OU performed the experiments. Authors OU, WBD, UIS, RKBD, OBD, Ramina and TSS performed literature survey and statistical analysis. All the authors wrote the protocol and first draft of the manuscript and managed the analyses of the study. Author TS collected X-ray diffraction data. All authors read and approved the final manuscript.

Article Information

DOI: 10.9734/CSJI/2019/v26i230091

Editor(s):

(1) Dr. T. P. West, Professor, Department of Chemistry, Texas A&M University-Commerce, USA.

Reviewers:

(1) Rodica Olar, University of Bucharest, Romania.

(2) Katalin Mészáros Szécsényi, University of Novi Sad, Serbia.

Complete Peer review History: <http://www.sdiarticle3.com/review-history/48127>

Original Research Article

Received 09 January 2019

Accepted 22 March 2019

Published 27 March 2019

ABSTRACT

(E)-1-((pyridin-2-yl)methylidene)semicarbazide (PMSC) complexes of $[\text{Mn}(\text{PMSC})_2] \text{Cl}_2$ (1), $[\text{Co}(\text{PMSC})_2] \text{Cl}_2$ (2), $[\text{Ni}(\text{PMSC})_2] \text{Cl}_2 \cdot 5\text{H}_2\text{O}$ (3), and $[\text{Cu}(\text{PMSC})(\text{H}_2\text{O})] \text{Cl}_2$ (4) have been synthesized and characterized by different spectroscopic techniques, EPR, magnetic susceptibility and thermal stability measurements. Complex 3 crystallizes as octahedral coordination complex in monoclinic crystal system. Complexes 1 and 2 have been found to have octahedral geometries and 4 to have square planar geometry. The complexes were found to be groove binding to calf-thymus DNA.

*Corresponding author: E-mail: bhubonsingh@gmail.com;

Keywords: Schiff base; complex; DNA; groove binding.

1. INTRODUCTION

Schiff Bases are widely interested due to their relevance in living system as in aminotransferase reactions [1], aldolase reactions [2], and in porphyrin biosynthesis [3] etc. Hydrazone-hydrazone Schiff bases have been considered novel bioactive molecules [4] because of their antitubercular [5-6], antimalarial [7], antimicrobial [8], analgesic and anti-inflammatory [9], antitumor [10-12] and other bioactivities [4]. Among them pyridine-2-carboxaldehyde thiosemicarbazones/semicarbazones and their metal complexes receive attention due to their ligation property and bioactivity [11-13]. The tumor-inhibitory activity of pyridine-2-carboxaldehyde thiosemicarbazone and 3-aminopyridine-2-carboxaldehyde thiosemicarbazone is reported due to their ability to inhibit metal binding site of Ribonucleotide Reductase, an iron dependent enzyme which catalyses the reduction of Ribonucleotide to Deoxyribonucleotide in the first step of DNA biosynthesis [12-13].

There are numerous reports on studies of transition metal complexes of pyridine-2-carboxaldehyde thiosemicarbazones [14-21]. However, reports on their semicarbazone analogues are very few. On pyridine-2-carboxaldehyde semicarbazone complexes it is worth to mention the spectroscopic characterization of pentacoordinated or octahedral Ni(Pysc) X_2 , Ni(Pysc) $_2X_2$, Co(Pysc) X_2 , Co(Pysc) $_2X_2$ (where X is uninegative anions) by Iskander et. al [14] and Co(L) $_2SO_4$ and Cu(L) $_2(SO_4)$ by Chandra and Kumar [21], and single crystal X-ray structures by Kasuga et. al. ([Ni(Hasc) $_2$](OAc) $_2$; Hasc = 2-acetylpyridine semicarbazone) [15], Zhao et. al. ([Ni(C $_7$ H $_8$ N $_4$ O) $_2$] [22], [Co(C $_7$ H $_8$ N $_4$ O) $_2$](ClO $_4$) $_2$ H $_2$ O [23]), Gerbelini et. al. ([FeII(HL) $_2$](ClO $_4$) $_2$ ·H $_2$ O, [CuII(HL) $_2$](ClO $_4$) $_2$ ·H $_2$ O [Ni(HSCpy) $_2$](ClO $_4$) $_2$ ·H $_2$ O, [Cu^{II}(HL)(H $_2$ O)(SO $_4$) $_n$], [Mn^{II}(HSCpy) $_2$](ClO $_4$) $_2$ ·C $_2$ H $_5$ OH) [24-27]. Of the reported complexes [14-15,21-27] their biologically activity is either not studied [14,21-27] or found inactive [15]. However Subashchandra bose et al based on theoretical studies predicted physical, chemical and biological applications of (E)-1-((pyridin-2-yl)methylidene)semicarbazide (PMSC) [28]. However, to best of our knowledge no biological studies have been carried out till date.

The interaction of transition metal complexes with DNA continues to attract interest in relation

to enzyme-DNA interaction and in the search for anticancer chemotherapeutic agents [29-37]. Transition metal complexes can bind to DNA *via* covalent and/or non-covalent interactions [29]. The labile ligand of metal complex such as chloride can be replaced by base nitrogen of DNA to form covalent bonds [29]. The non-covalent DNA interactions include (1) electrostatic interaction with the phosphates, (2) intercalative insertion between base pairs, and (3) groove binding [32-37].

In view of above importance and in continuation of our research in the field of biologically active complexes [30-33], we herein report the syntheses, spectroscopic characterization and DNA binding studies of Mn(II), Co(II), Ni(II) and Cu(II) (E)-1-((pyridin-2-yl)methylidene)semicarbazide (PMSC) complexes.

2. MATERIALS AND METHODS

2.1 Materials and Physical Techniques

All the chemicals were purchased from Sigma Aldrich and Himedia and used as received without further purification. Elemental (C, H, N) analysis were carried out using Perkin Elmer 2400 II Elemental Analyzer. FTIR spectra (KBr pellets, 4000-400 cm⁻¹) were recorded on a Shimadzu FTIR-8400 S spectrometer. NMR spectra were recorded by using Bruker AV III 500 MHz spectrometer and Mass spectra were recorded with WATER (ZQ-4000) Mass spectrophotometer. UV-vis spectra as well as the absorption titration studies were recorded on Perkin Elmer Lambda 35 UV/VIS spectrometer. Perkin Elmer LS 55 Fluorescence spectrophotometer was used in Ethidium bromide-DNA fluorescence quenching experiment. Cyclic voltammetry measurements were carried out using a CHI602C Electrochemical Analyzer against Ag/AgCl (saturated KCl) reference electrode with glassy carbon working electrode and Pt-wire counter electrode. JEOL, JES-FA200 ESR spectrometer was used to record EPR spectra at RT and at LNT. Sherwood Scientific Magnetic Susceptibility Balance (MSB) calibrated with mercury(II) tetrathiocyanatocobaltate(III) was used to measure RT magnetic susceptibilities. The thermograms were recorded on Perkin Elmer STA 6000 Simultaneous Thermal Analyzer using 10 mg each for complexes 1, 2, 3 and 7 mg for 4 within temperature range 30 to 800°C in N $_2$ atmosphere at a heating rate of 10°C min⁻¹.

Viscosity measurements in DNA binding studies were carried out using Ostwald's viscometer immersed in a thermostated water bath at 298 K. The viscosities (η) of samples were determined using the equation $\eta = (t - t_0)/t_0$ where t_0 is the flow time of buffer alone and t is the flow time of CTDNA solutions with increasing concentrations of complex.

2.2 Synthesis of Ligand and Complexes

2.2.1 Synthesis of (E)-1-((pyridin-2-yl)methylidene)semicarbazide (PMSC) ligand

The PMSC ligand was prepared as purple colored crystalline solid by refluxing 2-Pyridinecarboxaldehyde (2 mmol, 0.190 mL) and semicarbazide hydrochloride (2 mmol, 0.222 g) in 20 mL of methanol for 2 hours. Crystalline solid ligand was collected by slow evaporation. Yield: 0.34 g (83%). mp ($^{\circ}\text{C}$): 118-120; Anal. Calcd. for $[\text{C}_7\text{H}_8\text{N}_4\text{O}]$: C, 51.21; H, 4.91; N, 34.12 %. Found: C, 51.15; H, 4.90; N, 34.11 %. FT-IR (KBr , cm^{-1}): 3210, 3160 ($-\text{NH}_2$), 1705 ($\text{C}=\text{O}$), 1665 ($\text{C}=\text{N}$).

2.2.2 Synthesis of $[\text{Mn}(\text{PMSC})_2]\text{Cl}_2$ (1), $[\text{Co}(\text{PMSC})_2]\text{Cl}_2$ (2), $[\text{Ni}(\text{PMSC})_2]\text{Cl}_2 \cdot 5\text{H}_2\text{O}$ (3), $[\text{Cu}(\text{PMSC})(\text{H}_2\text{O})]\text{Cl}_2$ (4)

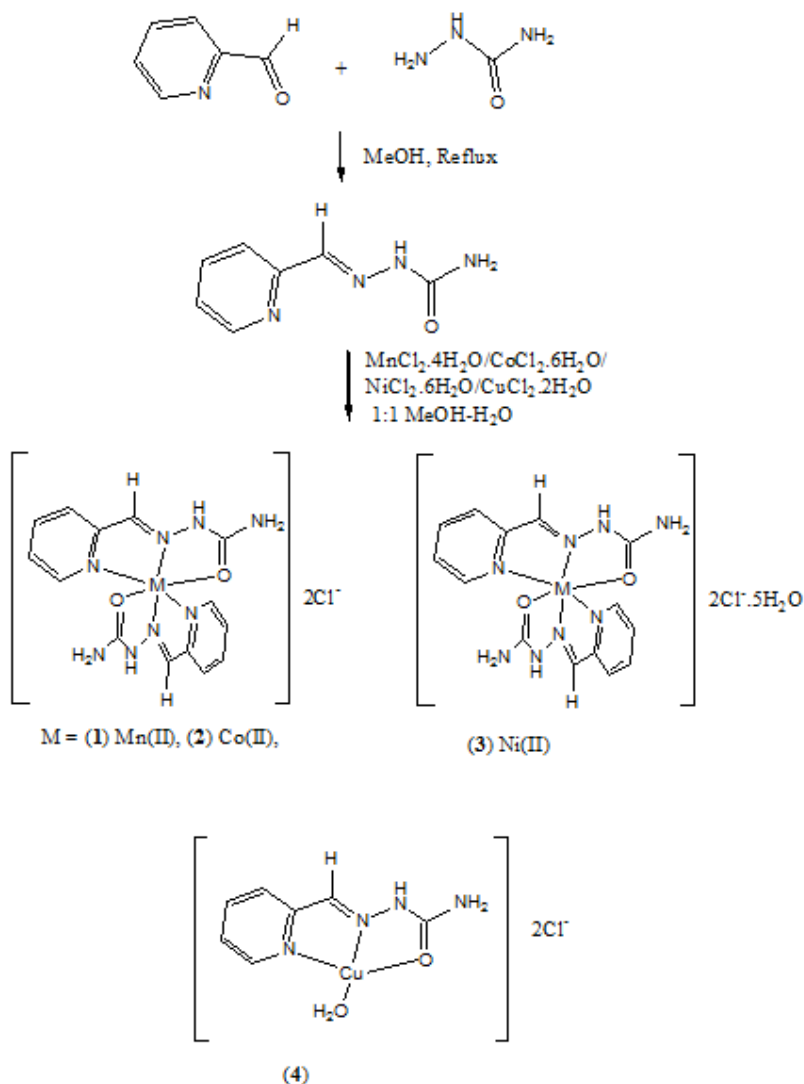
The complexes 1 to 4 were synthesized using metal to Schiff base ligand ratio of 1:2. They were prepared by adding drop wise metal chloride ($\text{MnCl}_2 \cdot 4\text{H}_2\text{O}$, $\text{CoCl}_2 \cdot 6\text{H}_2\text{O}$, $\text{NiCl}_2 \cdot 6\text{H}_2\text{O}$, $\text{CuCl}_2 \cdot 2\text{H}_2\text{O}$) solution (0.5 mmol) in 10 mL 1:1 methanol-water to stirring solution of PMSC (1 mmol, 0.164 g) in 10 mL 1:1 water-methanol. On slow evaporation complex 3 crystallized and the green colored single crystals were collected after one week. The crystalline precipitate obtained on slow evaporation of 1, 2, and 4 were filtered, washed with ethanol and collected for analysis.

- 1) Yield: 0.14 g (55%), Anal. Calc. for $[\text{Mn}(\text{PMSC})_2]\text{Cl}_2$: C, 37.02; H, 3.55; N, 24.67%. Found: C, 37.00; H, 3.52, N, 24.66%; UV-vis [nm ($\text{M}^{-1}\text{cm}^{-1}$)]: 525 (0.05), 305 (1.00); FT-IR (KBr , cm^{-1}): 3187, 3122 ($-\text{NH}_2$), 1685 ($\text{C}=\text{O}$), 1653 ($\text{C}=\text{N}$), 565 ($\text{Mn}-\text{N}$), 453 ($\text{Mn}-\text{O}$); EI-MS (70eV): $m/z = 383.21$ [M^+], 219.10 [base peak]; $^1\text{HNMR}$ ($\text{DMSO}-d_6$): $\delta = 12.83, 12.34$ (2H, $-\text{NH}_2$), 9.32 (1H, s, $-\text{NH}-$), 8.45 (1H, s, $=\text{CH}-$), 8.06 to 7.46 (4H, m, ArH); Magnetic moment (27°C , μ_B), 5.7; Λ_M (Acetonitrile, 27°C , $\text{S cm}^{-1}\text{M}^{-1}$): 141.

- 2) Yield: 0.16 g (60%), Anal. Calc. for $[\text{Co}(\text{PMSC})_2]\text{Cl}_2$: C, 36.70, H, 3.52, N, 24.45%. Found: C, 36.70, H, 3.50, N, 24.43%. UV-vis [nm ($\text{M}^{-1}\text{cm}^{-1}$)]: 525 (0.20), 305 (3.00); FT-IR (KBr , cm^{-1}): 3167, 3098 ($-\text{NH}_2$), 1702 ($\text{C}=\text{O}$), 1618 ($\text{C}=\text{N}$), 512 ($\text{Co}-\text{N}$), 458 ($\text{Co}-\text{O}$); $^1\text{HNMR}$ ($\text{DMSO}-d_6$): $\delta = 12.34, 11.44$ (2H, $-\text{NH}_2$), 10.12 (1H, s, $-\text{NH}$), 9.05 (1H, s, $=\text{CH}-$), 8.64 to 7.77 (4H, m, ArH); EI-MS (70eV): $m/z = 387.35$ [M^+], 223.10 [base peak]; Magnetic moment (27°C , μ_B), 3.98; Λ_M (Acetonitrile, 27°C , $\text{S cm}^{-1}\text{M}^{-1}$): 146.
- 3) Yield: 0.14 g (50%), Anal. Calc. for $[\text{Ni}(\text{PMSC})_2]\text{Cl}_2 \cdot 5\text{H}_2\text{O}$: C, 30.68, H, 4.78, N, 24.45%. Found: C, 30.67; H, 4.75, N, 24.42%; UV-vis [nm ($\text{M}^{-1}\text{cm}^{-1}$)]: 890 (0.08), 691 (0.07), 387 (2.5); FT-IR (KBr , cm^{-1}): 3039, 3010 ($-\text{NH}_2$), 1610 ($\text{C}=\text{O}$), 1505 ($\text{C}=\text{N}$), 539 ($\text{Cu}-\text{N}$), 455 ($\text{Cu}-\text{O}$); Magnetic moment (27°C , μ_B), 2.87; Λ_M (Acetonitrile, 27°C , $\text{S cm}^{-1}\text{M}^{-1}$): 120.
- 4) Yield: 0.06 g (75%), Anal. Calc. for $[\text{Cu}(\text{PMSC})(\text{H}_2\text{O})]\text{Cl}_2$: C, 26.55, H, 3.18, N, 17.69%. Found: C, 26.54, H, 3.15, N, 17.64%; UV-vis [nm ($\text{M}^{-1}\text{cm}^{-1}$)]: 840 (0.20), 307 (2.20); FT-IR (KBr , cm^{-1}): 3281, 3157 ($-\text{NH}_2$), 1674 ($\text{C}=\text{O}$), 1631 ($\text{C}=\text{N}$), 558 ($\text{Cu}-\text{N}$), 515 ($\text{Cu}-\text{O}$); EI-MS (70 eV): $^1\text{HNMR}$ ($\text{DMSO}-d_6$): $\delta = 13.18, 12.55$ (2 H, $-\text{NH}_2$), 10.49 (1H, s, $-\text{NH}-$), 8.51 (1 H, s, $=\text{CH}-$), 8.14 to 7.31 (4 H, m, ArH), 6.60 (2H, $-\text{H}_2\text{O}$); $m/z = 245.71$ [M^+], 81.94 [base peak]; Magnetic moment (27°C , μ_B), 1.68; Λ_M (Acetonitrile, 27°C , $\text{S cm}^{-1}\text{M}^{-1}$): 134.

2.3 Crystallographic Data Collection and Refinement

X-ray crystallographic data were collected on Xcalibur, Eos diffractometer equipped with graphite monochromatized $\text{Mo K}\alpha$ radiation ($\lambda = 0.7107 \text{ \AA}$) at 298 K. Data reduction and absorption correction were performed with CrysAlisPro, Agilent Technologies, Version 1.17.1.36.21. [38]. The structures were solved using SHELXL-2008 [39] and refined with full-matrix-least-squares on F^2 . Empirical absorption correction using spherical harmonics were implemented in SCALE3 ABSPACK scaling algorithm. Primary atoms were located by structure-invariant direct method. Hydrogen atom sites were inferred from neighboring sites. Molecular structure and crystallographic illustrations were prepared using OLEX-2 [40].



Scheme1. Reaction Scheme for Synthesis complex (1) to (4)

2.4 DNA-Binding Studies

For predicting the mode of CT-DNA binding of the newly synthesized complexes, Electronic absorption titrations, Fluorescence quenching experiment, Cyclic Voltammetric measurements and viscosity measurements were carried out.

3. RESULTS AND DISCUSSION

The Schiff base ligand was synthesized by Schiff base condensation method. The reported complexes of the ligands were prepared by reaction with their respective metal salts (Scheme 1). The complexes are soluble in water

and other polar solvents. Molar conductances (Λ_M) of complexes 1 to 4 in acetonitrile at 27°C were found as 141, 146, 120 and 134 $\text{S cm}^{-1} \text{M}^{-1}$ respectively, showing 1:2 electrolytic in nature.

3.1 X-ray Diffraction Studies of 3

The complex (3), $\text{C}_{14}\text{H}_{26}\text{Cl}_2\text{N}_8\text{NiO}_7$ or $[\text{Ni}(\text{PMSC})_2]\text{Cl}_2 \cdot 5\text{H}_2\text{O}$ crystallizes in monoclinic space group $\text{P}2_1/a$ in octahedral geometry (Fig. 1(a)). The crystal data, selected bond angle and bond length are given in Table 1-3. In the complex two tridentate ketonic form of PMSC ligands, which possess *E* configuration with respect to imine double bond, meridionally

coordinate to the Ni⁺² center through N(pyridine), N(imine) and O(amide). The bond lengths Ni1-N1 [2.094(2) Å], Ni1-N5 [2.089(2) Å], Ni1-N2 [1.9835(19) Å], Ni1-N6 [1.9903(19) Å], Ni-O1 [2.0849(18) Å], Ni1-O2 [2.1313(17) Å] are comparable to earlier reported Ni-N(pyridine), Ni-N(imine) and Ni-O(amide) bonds for other nickel(II) complexes with semicarbazone ligands [25]. The Ni1-N1(pyridine) and Ni1-N5(pyridine) bonds are longer than Ni-N2(imine) and Ni1-N6(imine) bonds. The C7-O1 [1.249(3) Å] and C14-O2 [1.255(3) Å] are comparable with other reported coordinated C=O double bonds [1.247(2) Å] [25]. The imine C6-N2 and C13-N6 bonds [1.276(3) Å] are much shorter than C7-N3 and C14-N7 bonds [1.378(3) and 1.372(3) Å respectively] showing ketonic form of the ligand. The coordination angle of N1-Ni1-N2 [78.38(8)°], N2-Ni1-O1 [77.66(7)°], N5-Ni1-N6 [78.59(8)°], N6-Ni1-O2 [76.73(7)°] are smaller than 90° and N1-Ni1-O1 [155.93(7)°], N5-Ni1-O2 [155.23(7)°] are significantly smaller than 180° showing the complex has distorted octahedral geometry. The +2 charge of the complex is balanced by two chloride anions. The coordination compound crystallizes in hydrated form with five water molecules. The crystal packing is stabilized by hydrogen bonds involving PMSC ligands, H₂O molecules and chloride anions (Fig.1 (b)).

3.2 FTIR, UV-Vis and Thermal studies of 3

3.2.1 FTIR spectral studies of 3

The FTIR spectra of 3 (supplemental information S-1) shows broad band at 3600-3000 cm⁻¹ which is due to lattice water overlapped with pyridine C-H stretching as well as H-bonded -NH₂ stretching. The bands at 3201 and 3142 cm⁻¹ could be assigned to asymmetric and symmetric stretching vibrations of -NH₂ (Table 4). The absorption at 3010 cm⁻¹ can be assigned to pyridine C-H stretching. C=O and C=N vibrations are observed at 1697 and 1653 cm⁻¹ respectively. The absorption band at 1583 cm⁻¹ can be assigned to bending vibration of lattice water. Absorption bands at 565 and 465 cm⁻¹ are assigned to M-N and M-O vibrations respectively. The observed lower -NH₂ absorption frequency of 3 compared to those of PMSC ligands (3210 and 3160 cm⁻¹ [28]) could be related to the possibly stronger H-bonding in complexes. The observed lower frequencies of ligated C=O and ligated C=N absorption compared to free PMSC ligand (ν (C=O) at 1705 cm⁻¹ and ν (C=N) at 1665 cm⁻¹ [28]) are due to elongation and weakening of C=O and C=N bonds on ligation.

Table 1. Crystal data and details of structure refinement for 3

Identification code	TS-UW9
Empirical formula	C ₁₄ H ₂₆ Cl ₂ N ₈ NiO ₇
Formula weight	548.04
Temperature/K	295(2)
Crystal system	monoclinic
Space group	P2 ₁ /a
a/Å	9.9970(5)
b/Å	19.4892(10)
c/Å	13.0244(7)
α /°	90.00
β /°	107.509(6)
γ /°	90.00
Volume/Å ³	2420.0(2)
Z	4
ρ_{calc} /cm ³	1.504
μ /mm ⁻¹	1.072
F(000)	1136.0
Crystal size/mm ³	0.7 × 0.4 × 0.1
Radiation	MoK α (λ = 0.71073)
2 θ range for data collection/°	7.74 to 50
Index ranges	-11 ≤ h ≤ 11, -23 ≤ k ≤ 23, -15 ≤ l ≤ 15
Reflections collected	17030
Independent reflections	4233 [R _{int} = 0.0344]
Data/restraints/parameters	4233/0/304
Goodness-of-fit on F ²	1.031
Final R indexes [I >= 2 σ (I)]	R ₁ = 0.0350, wR ₂ = 0.0828
Final R indexes [all data]	R ₁ = 0.0477, wR ₂ = 0.0879
Largest diff. peak/hole / e Å ⁻³	0.41/-0.35

3.2.2 UV-Vis spectral studies of 3

The UV-Vis spectrum of 3 obtained in aqueous solution shows three transitions at 890 nm (11235 cm⁻¹, ϵ = 0.08 M⁻¹ cm⁻¹), 691 nm (14471 cm⁻¹, ϵ = 0.07 M⁻¹ cm⁻¹), 387 nm and (25839 cm⁻¹, ϵ = 2.50 M⁻¹ cm⁻¹) which can be assigned to spin allowed transitions ${}^3T_{2g} \leftarrow {}^3A_{2g}$, ${}^3T_{1g} \leftarrow {}^3A_{2g}$, and ${}^3T_{1g}(P) \leftarrow {}^3A_{2g}$ respectively of d⁸ pseudo-octahedral Ni(II) complexes (S-2 (e-f)) [41-42].

3.2.3 Thermal studies of 3

TGA curve of 3 (S-3) shows a gradual 60% weight loss in the temperature range 110 to 310°C which could be related to simultaneous loss of five lattice H₂O molecules, 2 Cl⁻ ions, and one PMSC ligand (calc. wt.% = 59.3). This is

followed by gradual weight loss of 25% weight loss at 320 to 640°C which could be related to the loss of second PMSC ligand (cal. wt. % = 29.9). The DTA curve of 3 shows a sharp endothermic peak at 120°C and a broad endothermic peak at 230°C possibly due to dehydration and loss of chloride counter ions and one PMSC ligand. The curve also shows a broad exothermic peak which centers at 590°C; this could be related to the loss of second PMSC ligand.

3.3 FTIR, UV-Vis, EPR, ESI-MS and ¹HNMR spectroscopic and Thermal studies of 1, 2 and 4

3.3.1 FTIR spectral studies

The FTIR spectra of 1, 2 and 4 (supplemental information S-1) show broad band at 3600-3000 cm⁻¹ which is due to lattice/coordinated water overlapped with pyridine C-H stretching as well as H-bonded -NH₂ stretching similar to that of 3. The asymmetric and symmetric stretching vibrations of -NH₂ are observed at 3187, 3122 (1), 3167, 3098 (2), and 3281, 3157 (4) cm⁻¹ (Table 4). The band at 3007 (1), 3003 (2), and 3005 (4) cm⁻¹ can be assigned to pyridine C-H stretching. The C=O stretching band is observed at 1685 (1), 1702 (2), and 1674 (4) cm⁻¹. The C=N stretching band is observed at 1653 (1), 1618 (2) and 1631 (4) cm⁻¹. The absorption band at 1598 (4) can be assigned to bending vibration of coordinated H₂O molecule. Bands at 565 (1), 512 (2), 565 (3), 558 (4) cm⁻¹ and 453 (1), 459 (2), 455 (3), and 515 (4) are tentatively assigned to M-N and M-O absorptions respectively. Similar to IR spectrum of 3 the -NH₂, C=O, and C=N frequencies of 1, 2 and 4 are observed at lower frequencies compared to those of free PMSC ligand.

Table 2. Selected Bond-lengths (Å) of 3

Bond	Length/Å
Ni1-O2	2.13(17)
Ni1-O1	2.08(18)
Ni1-N5	2.08(2)
Ni1-N1	2.09(2)
Ni1-N2	1.98(19)
Ni1-N6	1.99(19)
O2-C14	1.25(3)
O1-C7	1.24(3)
N5-C12	1.35(3)
N5-C8	1.32(3)
N1-C5	1.35(3)
N1-C1	1.33(3)
C5-C4	1.379(3)

Table 3. Selected bond angles (°) of 3

Bond	Angle/°
O1-Ni1-O2	90.47(7)
O1-Ni1-N5	93.61(8)
O1-Ni1-N1	155.93(7)
N5-Ni1-O2	155.23(7)
N5-Ni1-N1	93.84(8)
N1-Ni1-O2	92.27(7)
N2-Ni1-O2	101.77(7)
N2-Ni1-O1	77.66(7)
N2-Ni1-N5	102.97(8)
N2-Ni1-N1	78.38(8)
N2-Ni1-N6	177.64(8)
N6-Ni1-O2	76.73(7)
N6-Ni1-O1	104.10(7)
N6-Ni1-N5	78.59(8)
N6-Ni1-N1	99.80(8)

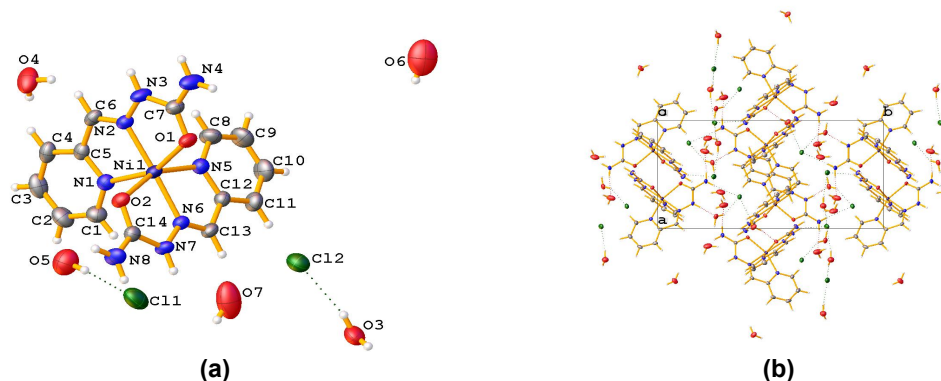


Fig. 1. (a) Crystal structure of 3 with atom numbering scheme having 50% ellipsoids (b) Packing diagram of complex 3 along c-axis

3.3.2 UV-Vis spectral studies

The UV-vis spectrum of pale pink colored 1 obtained in aqueous solution shows absorption bands at 525 nm (19047 cm^{-1} , $\epsilon = 0.05 \text{ M}^{-1} \text{ cm}^{-1}$) which may be assigned to spin forbidden sextet-quartet transition (${}^4T_{1g}(G) \leftarrow {}^6A_{1g}(S)$) of high spin Mn(II) octahedral complexes (S-2 (a-b)) [41]. Complex 2 shows an absorption at 525 nm (19047 cm^{-1} , $\epsilon = 0.20 \text{ M}^{-1} \text{ cm}^{-1}$) which may be assigned to ${}^4T_{1g}(P) \leftarrow {}^4T_{1g}(F)$ of high spin octahedral Co(II) complex (S-2 (c-d)) [41-42]. Complex 4 shows unresolved broad absorption band which centers around 840 nm (11904 cm^{-1} , $\epsilon = 2.10 \text{ M}^{-1} \text{ cm}^{-1}$) which is characteristic of square planar Cu(II) complexes (S-2 (g-h)) [43].

3.3.3 Mass spectral studies of complexes 1, 2 and 4

The ESI-MS spectral studies have been performed to determine the composition of the complexes 1, 2 and 4 in MeOH (Fig.2). The spectral analysis of 1 shows a base peak at m/z value 219.12 which matches well with the calculated m/z value of $[\text{Mn}(\text{PMSC})]^+$ (calc. 219.10) [44]. The peak at 383.21 may be assigned to $[\text{Mn}(\text{PMSC})_2]^+$ (calc. 383.27) [44]. Similar peaks are observed for 2, base peak at m/z 223.10 corresponding to $[\text{Co}(\text{PMSC})]^+$ (223.10) and another peak at 387.25 corresponding to $[\text{Co}(\text{PMSC})_2]^+$ (calc. 387.26) [44]. The mass spectral analysis of complex 4 shows base peak at m/z 81.94 which matches well with $[\text{Cu}(\text{H}_2\text{O})]^+$ (calculated 81.56) [44]. The spectra also shows a peak at m/z 245.71 which corresponds to m/z of $[\text{Cu}(\text{PMSC})(\text{H}_2\text{O})]^+$ (calc. 245.71) [44]. Free metal ion peaks are visible in all the spectra [44].

3.3.4 ${}^1\text{H}$ NMR spectral studies of 1, 2 and 4

The ${}^1\text{H}$ NMR spectra of 1 recorded in DMSO- d_6 solution at room temperature using tetramethylsilane as internal standard shows two broad signals at $\delta = 12.83, 12.34$ (2H) due to presence of $-\text{NH}_2$ (Fig. 3). The signals at $\delta = 9.32$ (1H, s) and $\delta = 8.15$ (1H, s) can be assigned to $-\text{NH}-$ and $=\text{CH}-$ respectively. The multiplet at $\delta = 8.06$ to 7.46 (m, 4H) is due to absorptions of aromatic ring hydrogen atoms ($-\text{ArH}$) [45]. Similar spectra of 2 shows $-\text{NH}_2$ at $\delta = 12.34$ and 11.44 (2H), $-\text{NH}-$ at $\delta = 10.12$ (1H), $=\text{CH}-$ at $\delta = 9.05$ (1H) and absorption of aromatic H atoms (ArH) at $\delta = 8.64$ to 7.77 (m, 4H) (Fig. 3). The spectra of 4 shows $-\text{NH}_2$ at $\delta = 13.18, 12.55$ (2H), $-\text{NH}$ at $\delta = 10.49$ (1H, s), $-\text{CH}=\text{C}$ at $\delta = 8.51$ (s, 1H) and aromatic ring hydrogen at $\delta = 8.14$ - 7.31 (m, 4H) ($-\text{ArH}$) (Fig. 3). The spectrum of 4 shows a broad absorption at $\delta = 6.60$ (s, 2H) which could be assigned to coordinated water; this signal is absent in the spectra of 1 and 2.

The EPR spectra of complex 1 recorded at room temperature in solid powder shows a band with isotropic $g = 2.00$ (Fig. 4 (a-b)) whereas frozen DMF solutions at 77 K, shows a hyperfine sextet with g value of 2.12, 2.06, 2.00, 1.94 and 1.82. This is due to the interaction of the electron spin with the nuclear spin ($I = 5/2$ for ${}^{55}\text{Mn}$, 100% abundance), a hyperfine sextet ($2n+1$ lines) is observed corresponding to $\Delta M_s = \pm 1$ and $\Delta M_l = 0$. The observed g value is very close to the free electron spin value of 2.0023, which is consistent with the typical manganese(II) system and also suggestive of the absence of spin orbit coupling in the ground state ${}^6A_{1g}$ [46].

3.3.5 EPR spectral studies

The polycrystalline solid EPR spectra of complex 2 at LNT (Fig.4 (c-d)) appear broad in the g value range 2.0 to 2.5 ($I=7/2$ for ${}^{59}\text{Co}$ – 100% abundance). The spectral feature shows 2 is a high spin ($S=3/2$) complex with considerable spin orbit coupling [46].

The hyperfine epr spectrum of 4 obtained in DMF at LNT, (Fig.4 (e-f)) is of characteristic mononuclear copper (II) complex. The trend $g_{\parallel} > g_{\perp} > 2.003$ indicates axial symmetry having $d_{x^2-y^2}$ ground state [47]. The g_{\parallel} value was found to be less than 2.29 indicating significant covalent character in metal ligand bonding [48]. Bonding parameters (α^2 , β^2 , γ^2) and orbital reduction factors (k_{\parallel} and k_{\perp}) were calculated from epr parameters (Table 5). The α^2 value was found to be 0.68 suggesting that there is about 32 % overlapping between ligand orbital and metal d-orbital [48]. The $k_{\parallel} > k_{\perp}$ showing the possibility of out-of-plane π bonding [47-48].

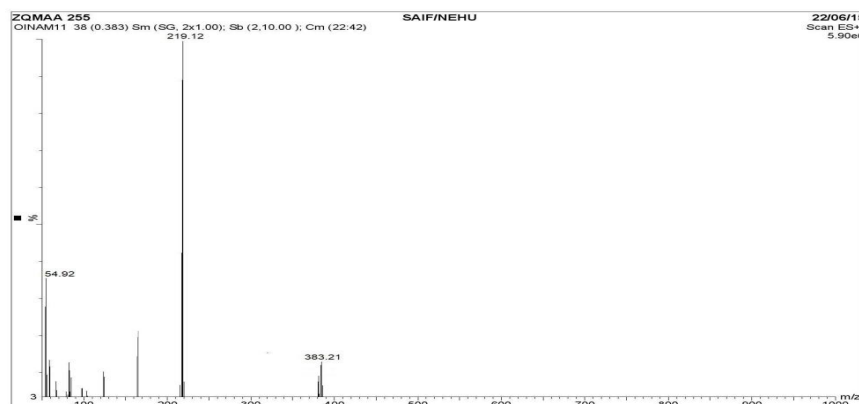
The thermal analyses of complexes are informative particularly to investigate the presence of coordinated/lattice water along with the composition of the complex. TGA curve of 1 (S-3) shows thermal stability of the complex up to 310°C followed by a 35% weight loss which could be related to the loss of counter ions and one PMSC ligand. It is followed by gradual loss of weight up to 700°C which can be related to

3.3.6 Thermal analysis

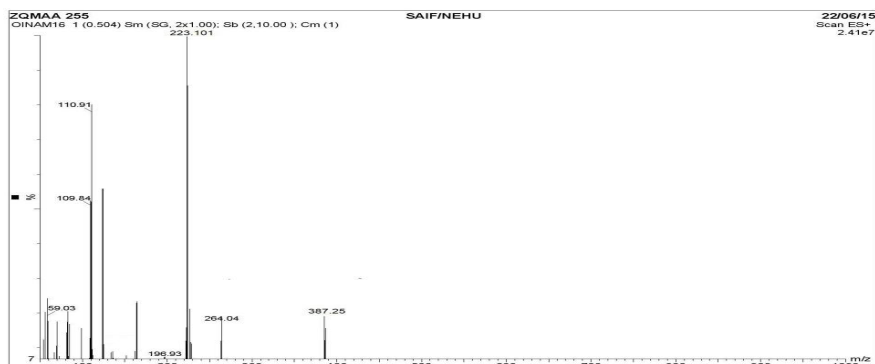
The thermal analyses of complexes are informative particularly to investigate the presence of coordinated/lattice water along with the composition of the complex. TGA curve of 1 (S-3) shows thermal stability of the complex up to 310°C followed by a 35% weight loss which could be related to the loss of counter ions and one PMSC ligand. It is followed by gradual loss of weight up to 700°C which can be related to

loss of another PMSC ligand. It shows exothermic peaks at 330 and 550°C related to successive loss of PMSC ligands. TGA curve of 2 shows 45% weight loss in the temperature range of 130 to 260°C which could be related to the loss of first PMSC ligand and counter ions which is followed by a gradual decrease in weight which continues up to 700°C due to loss of second PMSC ligand. In the DTA curve of 2 there is a

sharp exothermic peak at 230°C corresponding to the loss first PMSC ligand. There is broad exothermic peaks at 380°C in the DTA curve of 2; these can be assigned to the decomposition of second PMSC ligand. TGA curve of 4 (S-3) shows stepwise weight losses within 180°C to 300°C which could be related to loss of coordinated water, loss of counter ions and PMSC ligand. It is followed by gradual loss in weight.



(1)



(2)



(4)

Fig. 2 Mass spectra of 1, 2 and to 4

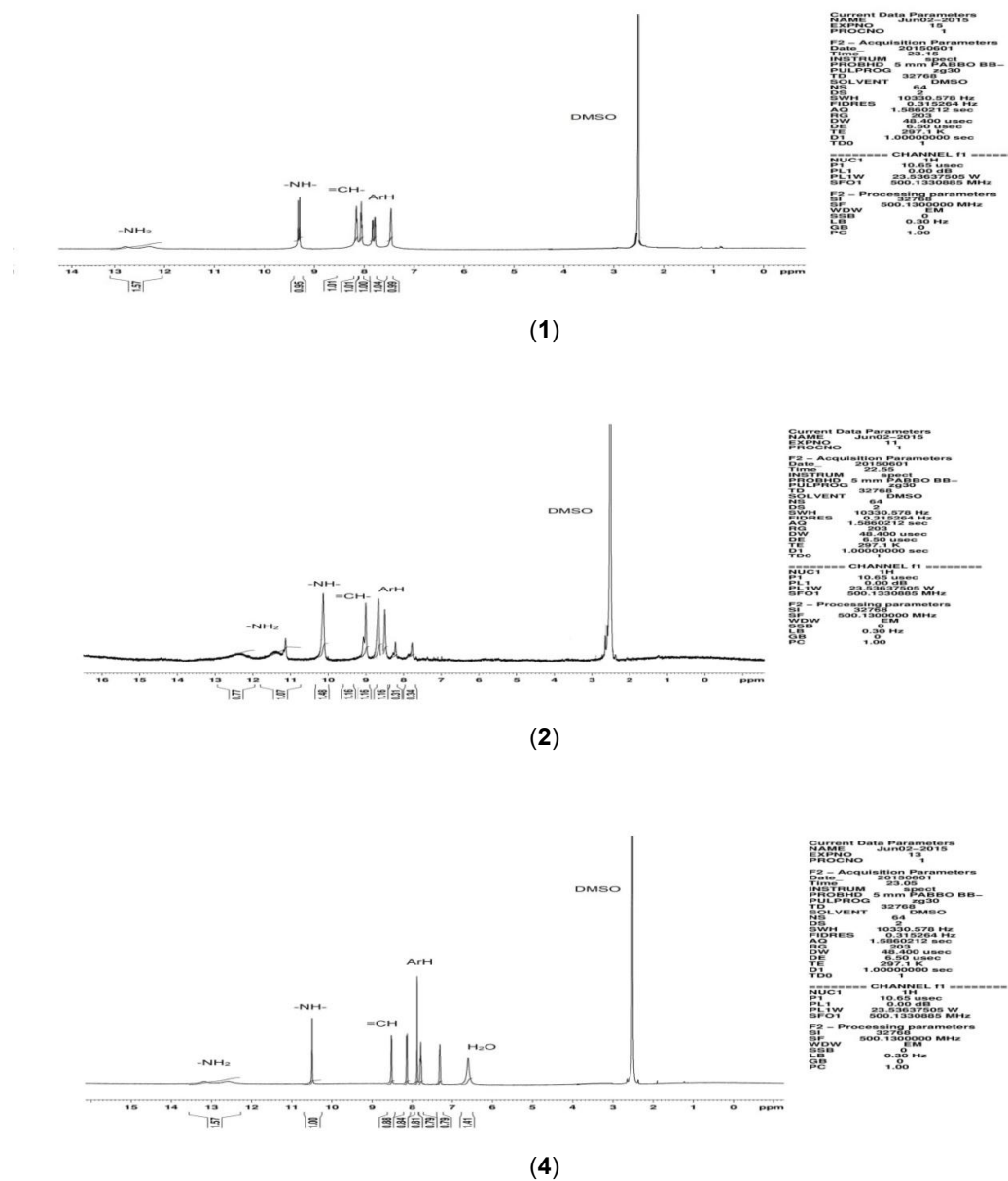


Fig. 3. ¹HNMR spectra of 1, 2 and 4 (from top to bottom)

Table 4. FTIR absorption frequencies (cm⁻¹) of complexes 1-4

ν (cm ⁻¹)	PMSC	1	2	3	4
-NH ₂ (as, s)	3210, 3160	3187, 3122	3167, 3098	3201, 3142	3281, 3157
C-H (py)	3010	3007	3003	3010	3005
>C=O	1705	1685	1702	1697	1674
>C=N-	1665	1653	1618	1653	1631
H ₂ O (bend)				1583	1598
M-N		565	512	565	558
M-O		453	458	455	515

Table 5. EPR bonding parameters of 4 in DMF at 77 K

E_{d-d} (nm)	$g_{ }$	g_{\perp}	g_{av}	$A_{ }$ (G)	A_{\perp} (G)	α^2	$k_{ }$	k_{\perp}	β^2	γ^2	G
840	2.29	2.05	2.14	120	12	0.68	0.72	0.58	1.05	0.85	5.8

$\alpha^2 = -(A_{||}/0.036) + (g_{||} - 2.0023) + 3(g_{\perp} - 2.0023)/7 + 0.04$; $k_{||}^2 = (g_{||} - 2.0023) E_{d-d} / 8\lambda_0$; $k_{\perp}^2 = (g_{\perp} - 2.0023) E_{d-d} / 2\lambda_0$; $k_{||} = \alpha^2 \beta^2$ and $k_{\perp} = \alpha^2 \gamma^2$; $G = (g_{||}-2)/(g_{\perp}-2)$. Here λ_0 is one electron spin orbit coupling constant and is equal to 828 cm^{-1}

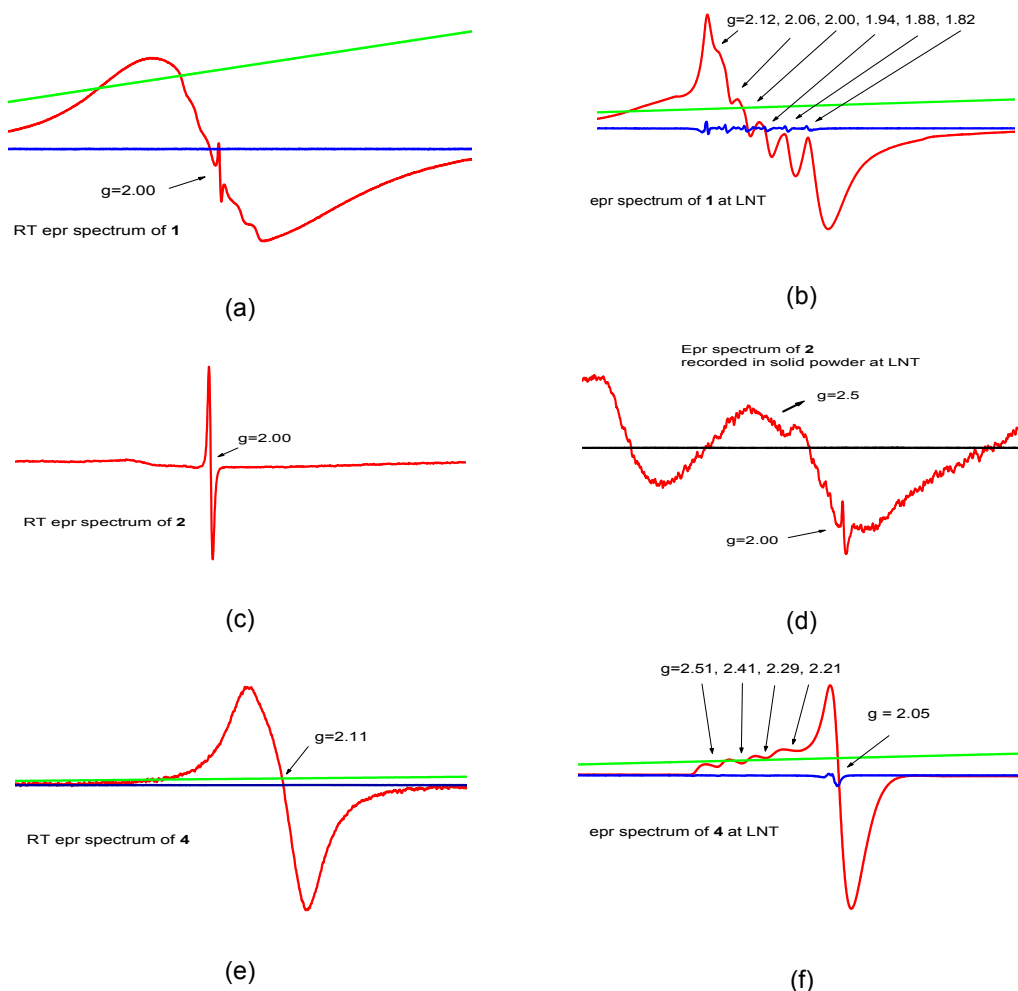


Fig. 4. EPR spectrum of 1 (a-b), 2 (c-d) and 4 (e-f) obtained from polycrystalline solid powder at room temperature (a, c, e) and from DMF solution at liquid nitrogen temperature (b, d, f)

3.4 DNA Binding Studies of 1 to 4

3.4.1 Electronic absorption titration

Electronic absorption titrations were carried out in tris buffer solution (pH = 7.2). The absorbance ratio of CT-DNA solution at 260 nm and 280 nm was found to be 1.9 suggesting that the CT-DNA

was satisfactorily free from protein [49]. The titrations were carried out by maintaining a constant concentration of the complex (5×10^{-4} M) and varying the concentration of CT-DNA solution added. The absorbance for each addition of CT-DNA was recorded subsequently. The intrinsic binding constant, K_b , for complexes 1 - 4 were determined by using equation (1),

$$[\text{DNA}]/(\epsilon_a - \epsilon_f) = [\text{DNA}]/(\epsilon_b - \epsilon_f) + 1/[K_b(\epsilon_b - \epsilon_f)] \quad (1)$$

Where, [DNA] is the concentration of DNA base pair which was calculated using molar absorption coefficient value $6600 \text{ M}^{-1} \text{ cm}^{-1}$ for DNA at 260 nm [50], the apparent absorption coefficients ϵ_a , ϵ_f , and ϵ_b corresponds to $A_{\text{obs}}/[\text{complex}]$, extinction coefficients of complex in free and bound state respectively. A plot of $[\text{DNA}]/(\epsilon_a - \epsilon_f)$ vs. [DNA] was used to calculate K_b from the ratio of slope and intercept [51].

The charge transfer (CT) bands of complex 1 (500 μM) in Tris-buffer solution at 250 and 277 nm displayed hypochromism in the presence of CT-DNA (0-100 μM) (Fig.5 (a)). The intrinsic binding constant was calculated using absorbance values at 277 nm.

The CT bands of complex 2 (500 μM) in Tris-buffer solution at 230 nm displayed hyperchromism in the presence of CT-DNA (0-100 μM) (Fig. 5 (c)). The absorbance values at 230 nm were used for calculating intrinsic binding constant.

The CT bands of complex 3 (500 μM) in Tris-buffer solution at 257 nm (Fig. 5 (e)) displayed hyperchromism in the presence of increasing concentration of CT-DNA (0-120 μM). The absorbance at 257 nm was used to calculate intrinsic binding constant.

The charge transfer bands of complex 4 (500 μM) in Tris-buffer solution at 273 nm (Fig. 5 (f)) displayed hypochromism in the presence of increasing concentration of CT-DNA (0-130 μM). The intrinsic binding constant of 4 was calculated using absorbance values at 273 nm.

The spectral patterns of complexes 1 to 4 were analogous to previously reported complexes whose interaction mode with DNA is non-intercalative and groove binding [30-33]. The intrinsic binding constant, K_b for each complex was determined from the plot of $[\text{DNA}] / (\epsilon_a - \epsilon_f)$ versus [DNA], (Fig. 5 (b, d, f, h)) using equation (1) in section 3.3.1. The slope to intercept ratio of the curves gave intrinsic binding constant K_b of 1.16, 2.38, 1.53 and $3.56 \times 10^4 \text{ M}^{-1}$ for complexes 1 to 4 respectively. The K_b values are lower than those observed for classical intercalators (ethidium-DNA, $1.4 \times 10^6 \text{ M}^{-1}$ in 40 mM Na^+ ion concentration in 25 mM Tris-HCl

(pH = 7.9) at 37°C [49-52]). The K_b values suggest weaker DNA binding affinity of the complexes than the classical intercalators [49-53]. From the observed results and finding the binding modes of the complexes were non-intercalative and groove or surface binding [30-33].

3.4.2 Fluorescence quenching experiment

Stock solution of CT-DNA was freshly prepared in 5 mM tris buffer (pH = 7.2), the ratio of absorbance at 260 nm and 280 nm was found to be 1.9 showing satisfactory protein free condition [49]. The concentration of the CT-DNA stock solution in tris buffer was calculated as $5 \times 10^{-4} \text{ M}$ using molar absorption coefficient value $6600 \text{ M}^{-1} \text{ cm}^{-1}$ of DNA at 258 nm [50]. Stock solutions of 1 to 4 in water ($5 \times 10^{-4} \text{ M}$) and stock solution of ethidium bromide (EB) in water (1.6 μM) were prepared. Appropriate dilutions of the stock solution were made for each experiment. In a typical experiment 2 mL each of ethidium bromide solution was transferred into a series of vials. 25 μL each of CT-DNA ($A_{260\text{nm}} = 2$) were added to the ethidium bromide solutions. To a DNA-EB solutions in different vials, different volumes of complex (0, 10, 20, 30, etc., μM) were added. A total volume of 2.5 mL in each solution was maintained by adding additional volume of buffer. The solutions were equilibrated for 15 min. The variation in the fluorescence intensities with increasing concentration of complex were recorded at 605 nm over a spectral range of 500 to 750 nm using an excitation wavelength of 546 nm. The apparent binding constant K_{app} was calculated from equation (2),

$$K_{\text{EB}}[\text{EB}] = K_{\text{app}}[\text{Complex}] \quad (2)$$

Where, $K_{\text{EB}} = 1.0 \times 10^7 \text{ M}^{-1}$, [EB] = 1.3 μM and [Complex] = the molar concentration of complex at 50% reduction of fluorescence [54]. The classical Stern-Volmer quenching constants (K_{SV}) were calculated for each complex using the plot of linear Stern-Volmer equation.

$$I_0/I = 1 + K_{\text{SV}}r \quad (3)$$

Where, I_0 and I are the fluorescence intensities of DNA-EB in the absence and presence of the complex respectively and r is the concentration ratio of complex to DNA [55-56]. K_{SV} value was obtained from the slope of a linear plot of I_0/I vs. r [56].

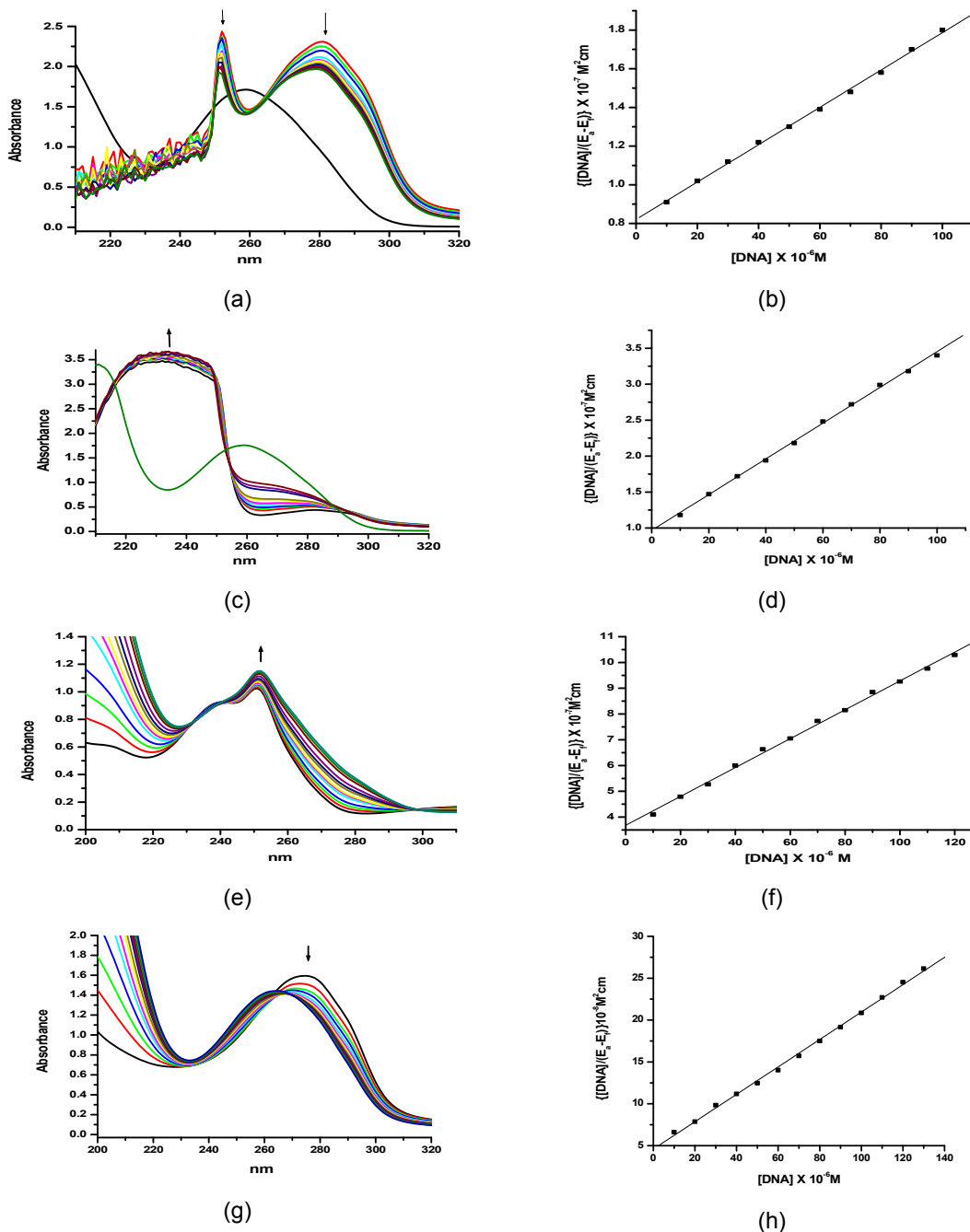


Fig. 5. Electronic absorption titration of 1 (a), 2 (c), 3 (e), 4 (g) (5×10^{-4} M) with CT-DNA (0-100 μM) in Tris-buffer (pH = 7.2). Plots of $[DNA] / (\epsilon_a - \epsilon_f)$ versus $[DNA]$ for complexes 1 (b), 2 (d), 3 (f), and 4 (h)

Ethidium bromide (EB) is a DNA intercalator [57] that gives significant fluorescence emission when intercalated between the adjacent DNA base pairs [53, 56]. The extent of fluorescence quenching for EB bound to DNA was used to study the extent of binding between the molecule

and DNA [53, 56, 58]. Fig. 6 (a, c, e, g) shows the reductions in the fluorescence emission intensities of EB-DNA (10 μM) with increasing concentration of complexes (0-100 μM) recorded in tris buffer solution (pH = 7.2). Using equation (2) the apparent binding constant K_{app} were

calculated as 3.2, 4.3, 6.5 and $3.2 \times 10^5 \text{ M}^{-1}$ for complex 1 to 4 respectively. The observed values of K_{app} suggested the complexes were binding towards CT-DNA [54]. The quenching of EB-DNA fluorescence by the complexes was in good agreement with the linear Stern-Volmer equation (3), (Fig.6 b, d, f, h) [53]. The slope of the linear plot I_0/I vs. r ($r = [\text{Complex}]/[\text{DNA}]$)

gave quenching constant K_{SV} values of 0.27, 0.20, 0.36 and 0.14 for complexes 1 to 4 respectively. The values suggested competitive inhibition caused by minor groove binding of complex, releasing some free EB from DNA-EB complex and blocking potential interaction sites of EB [53,56,59].

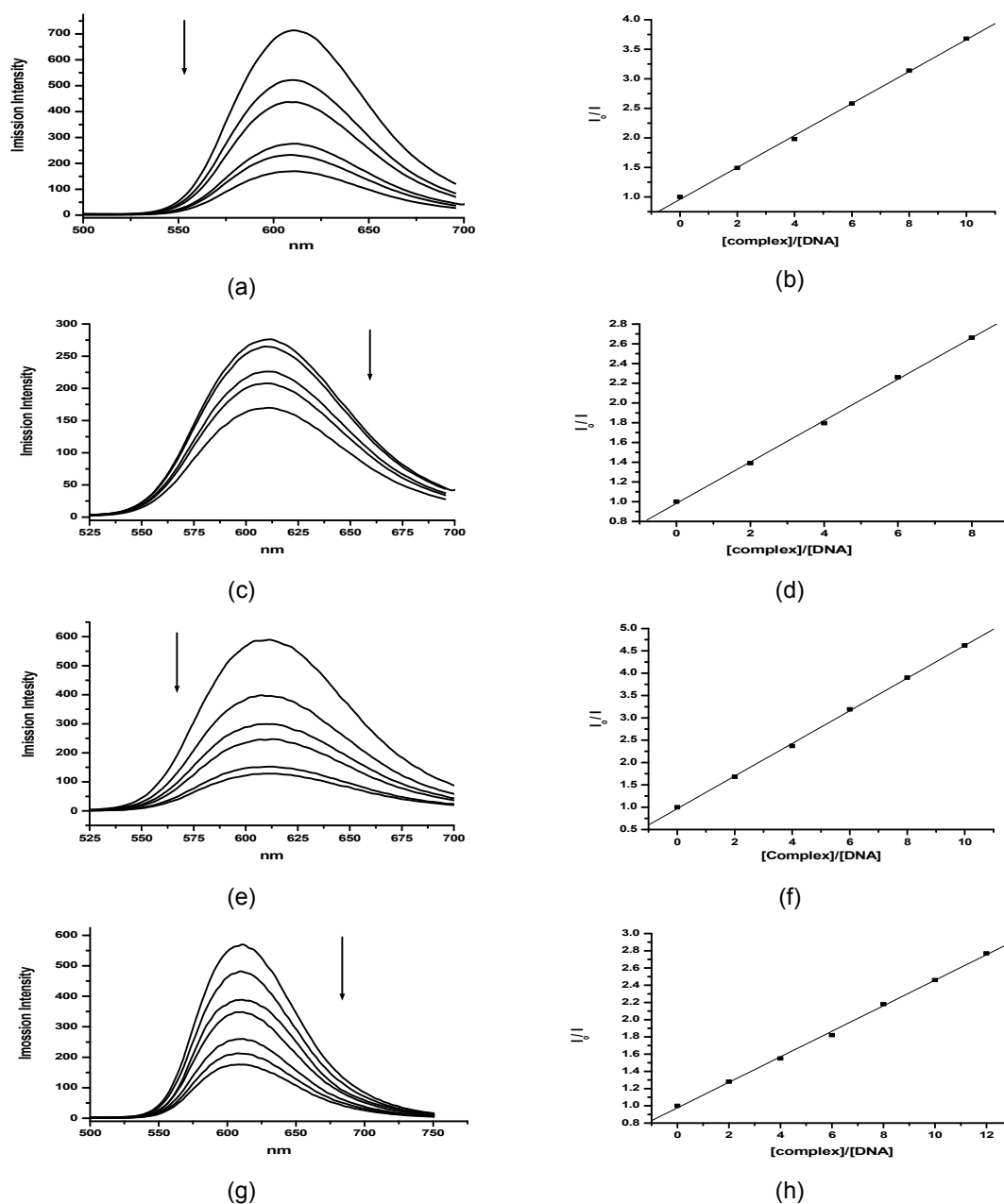


Fig. 6. Fluorescence emission spectra of Ethidium bromide-CTDNA in Tris-HCl buffer (pH = 7.2) with increasing concentration of 1 (a), 2 (c), 3 (e) 4 (g); $\lambda_{ex} = 546 \text{ nm}$. Fluorescence quenching curve of EB-DNA by 1 (b), 2 (d), 3 (f) and 4 (h)

3.4.3 Cyclic voltammetry

The room temperature cyclic voltammogram of complex 1 to 4 (50 μ M) vs. AgCl/Ag (saturated KCl) within +1.0 V to -1.0 V at a scan rate of 0.01 V/s in Tris-buffer (pH =7.2) in the absence and presence of CT-DNA (5×10^{-4} M) are given in Fig. 7. The cyclic voltammetric parameters of the complexes are given in Table 6.

Cyclic voltammogram of 1 in the absence of DNA gave two reduction peaks at 0.27 and -0.54 V (Fig. 7) which may be assigned to reduction of Mn(IV) to Mn(III) and Mn(III) to Mn(II) respectively [60]. The oxidation peaks observed at 0.38 and 0.68 V can be assigned to oxidation of Mn(II) to Mn(III) and Mn(III) to Mn(IV) respectively [60]. In the presence of CT-DNA two reduction peaks 0.28 V [Mn(IV)/Mn(III)], -0.60 V [Mn(III)/Mn(II)] and two oxidation peaks 0.60 V [Mn(II)/Mn(III)] and 0.75 V [Mn(III)/Mn(IV)] were observed. The formal potential $E_{1/2}$ values [-0.08 and 0.47 V] of 1 were shifted to more positive values [0.0 and 0.51 V] in the presence of CT-DNA (Table 6).

The CV of 2 (Fig. 7) gave a reduction peak at -0.62 V and an oxidation peak at 0.37 V. The reduction peak could be assigned to reduction of Co(II) to Co(I) and oxidation peak could be assigned to oxidation of Co(I) to Co(II) [61]. In the presence of CT-DNA the reduction and oxidation peaks were observed at -0.71 and 0.39 V respectively. The formal potential $E_{1/2}$ value -0.12 V of 2 was shifted to more negative value -0.16 V in the presence of CT-DNA.

The CV of 3 (Fig. 7) gave a reduction peak at -0.37 V which could be assigned to reduction of Ni(II) to Ni(I) [62]. The oxidation peak of 3

observed at 0.50 V could be assigned to oxidation of Ni(I) to Ni(II) [62]. In the presence of CT-DNA the reduction and oxidation peaks were observed at -0.42 and 0.50 V respectively. The formal potential $E_{1/2}$ value 0.06 V of 3 was shifted to more negative value 0.04 V in the presence of DNA.

The cyclic voltammogram of 4 (Fig. 7) gave a reduction peak at -0.99 V which could be assigned to reduction of Cu(II) to Cu(I) [61]. The oxidation peak of 4 observed at 0.29 V could be assigned to oxidation of Cu(I) to Cu(II) [61]. In the presence of CT-DNA the reduction and oxidation peaks were observed at -0.85 and 0.19 V respectively. The formal potential $E_{1/2}$ value -0.35 V of 4 was shifted to more positive value -0.33 V in the presence of CT-DNA.

For all the complexes the peak separation values and peak current ratios shows that the redox processes are not reversible. As the DNA and the respective ligands did not show any redox processes it can be concluded that the redox processes are due to metal centers. The overall experimental suggests that the presence of DNA strongly affects the redox processes of metal centers in all the complexes.

Among the three kinds of binding modes of small molecules to DNA, if the formal potential $E_{1/2}$ is shifted to more positive value the interaction mode is intercalative binding, while $E_{1/2}$ shifted to more negative value the binding mode is electrostatic [56]. It has been observed that the shift in $E_{1/2}$ values in presence of DNA from that in the absence of DNA are insignificant, suggesting the complexes bind to CT-DNA by surface or groove binding mode.

Table 6. Cyclic voltammetry data for 1 - 4 in the absence and presence of CT-DNA^a

complex	E_{pa} (V)	$i_{pa} \times 10^5$ A	E_{pc} (V)	$i_{pc} \times 10^5$ A	ΔE (V)	i_{pa}/i_{pc}	$E_{1/2}$ (V)
1	0.38	-8.93	-0.54	5.83	0.92	1.53	-0.08
	0.68	-9.91	0.27	7.10	0.21	1.39	0.47
1 + DNA	0.60	-8.93	-0.60	4.55	1.20	1.96	0.0
	0.75	-9.97	0.28	6.58	0.47	1.51	0.51
2	0.37	-4.75	-0.62	4.19	0.99	1.13	-0.12
2 + DNA	0.39	-2.97	-0.71	2.42	1.10	1.22	-0.16
3	0.50	-8.17	-0.37	7.63	0.87	1.07	0.06
3 + DNA	0.50	-7.65	-0.42	7.45	0.92	1.02	0.04
4	0.29	-3.06	-0.99	2.33	1.28	1.31	-0.35
4 + DNA	0.19	-1.90	-0.85	1.46	1.04	1.30	-0.33

^a E_{pa} , i_{pa} and E_{pc} , i_{pc} are anodic and cathodic peak potentials and peak currents; $\Delta E = E_{pa} - E_{pc}$ and $E_{1/2} = (E_{pa} + E_{pc})/2$

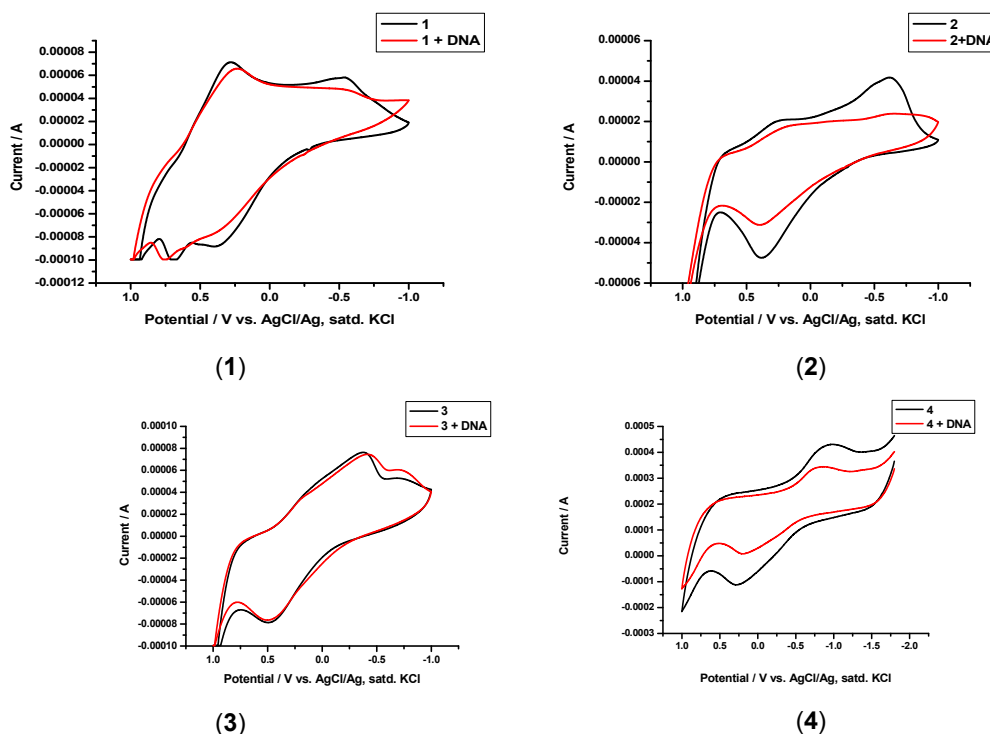


Fig. 7. Cyclic voltammogram of 1-4 (50 μM) against AgCl/Ag (saturated KCl) electrode within +1 V to -1 V at a scan rate of 0.01V/s in the absence (black) and presence (red) of CT-DNA (5×10^{-4} M)

3.4.5 Viscosity measurements

Viscosity measurement of DNA solution with increasing concentrations of complex is useful for determining the binding mode of interaction of complex with DNA. The effects of small molecules- bound to DNA with different modes of binding- on viscosity of DNA solution are as follows: Intercalative binding causes an increase in viscosity, non-classical intercalative binding causes a lowering in viscosity and surface or groove binding causes no change in viscosity of CT-DNA solution [31]. When viscosities of DNA solutions with increasing concentrations of the complexes 1 to 4 were measured the relative viscosities (η/η_0) were found to be unchanged suggesting that the complexes bind with DNA via non-intercalative surface or groove binding.

4. CONCLUSION

The present work reports on the synthesis, spectroscopic characterization and DNA binding studies of (E)-1-((pyridin-2-yl)methylidene)semicarbazide complexes of

Mn(II), Co(II), Ni(II) and Cu(II). X-ray diffraction study shows that 3 has octahedral geometry in which two tridentate ketonic form of PMSC ligands, which possess *E* configuration with respect to imine double bond, meridionally coordinate to the Ni⁺² center through N(pyridine), N(imine) and O(amide). Different spectroscopic techniques, magnetic susceptibility measurements and thermal analysis shows that complexes 1 and 2, have octahedral coordination environments while complex 4 has square planar coordination environment. Electronic absorption titration experiment, EB-DNA fluorescence quenching experiments, cyclic voltammetric experiments and viscosity measurements suggests that the complexes might be non-intercalative surface or groove binder to CT-DNA.

ACKNOWLEDGEMENTS

This work has been carried out with the financial support of University Grants Commission (UGC), New Delhi. The support was gratefully acknowledged.

SUPPLEMENTARY MATERIALS

CCDC No. 1575938 contains the supplementary crystallographic data reported in this paper. These data can be obtained free from www.ccdc.cam.ac.uk/data_request/cif

COMPETING INTERESTS

Authors have declared that no competing interests exist.

REFERENCES

1. Toney MD. Aspartate aminotransferase: an old dog teaches new tricks. *Arch. Biochem. Biophys.* 2014;119-127. DOI: 10.1016/j.abb.2013.10.002
2. Tittmann K, Sweet siblings with different faces: The mechanism of FBP and F6P aldolase, transaldolase, transketolase revisited in the light of recent structural data. *Bioorg. Chem.* 2014. DOI: 10.1016/j.bioorg.2014.09.001
3. Leeper FJ. The biosynthesis of porphyrins, chlorophylls, and vitamin B₁₂. *Nat. Prod. Rep.* 1985;2:19-47. DOI: 10.1039/NP9850200019
4. Rollas S, Küçükgüzel ŞG. Biological Activities of Hydrazone Derivatives. *Molecules.* 2007;12:1910-1939. DOI: 10.3390/12081910
5. Pavan FR, Maia PI, da S, Leite SRA, Deflon VM, Batista AA, Sato DN, Franzblau SG, Leite CQF. Thiosemicarbazone, semicarbazone, dithiocarbazates and hydrazide/hydrazones: Anti-mycobacterium tuberculosis activity and cytotoxicity. *Eur. J. Med. Chem.* 2010;45:1898-1905. DOI: 10.1016/j.ejmech.2010.01.028
6. Jamadar A, Duhme-Klair AK, Vemuri K, Sritharan M, Dandawate P, Padhye S. Synthesis, characterisation and antitubercular activities of a series of pyruvate-containing aroylhydrazones and their Cu-complexes. *J. Chem. Soc., Dalton Trans.* 2012;41:9192-9201. DOI: 10.1039/c2dt30322a
7. Arai M, Alavi YIH, Mendoza J, Billker O, Senden RE. Isonicotinic acid hydrazide: An anti-tuberculosis drug inhibits malarial transmission in mosquito gut. *experimental parasitology.* 2004;106:30-36. DOI: 10.1016/j.exppara.2004.01.002
8. Popiolek L. Hydrazide-hydrazones as potential antimicrobial agents: Overview of the literature since 2010. *Med. Chem. Res.* 2017;26:287-301. DOI: 10.1007/s00044-016-1756-y
9. Rineh A, Mahmoodi N, Abdollahi M, Foroumadi A, Sorkhi M, Shafiee A. Synthesis, analgesic and anti-inflammatory activity of 4-(2-Phenoxyphenyl)semicarbazones. *Arch. Pharm. Chem. LifeSci.* 2007;340:409-415. DOI: 10.1002/ardp.200700045
10. Mohareb RM, Fleita DH, Sakka OK. Novel synthesis of hydrazide-hydrazone derivatives and their utilization in the synthesis of coumarin, pyridine, thiazole and thiophene derivatives with antitumor activity. *Molecules* 2011;16:16-27. DOI: 10.3390/molecules16010016
11. Antholine W, Taketa F. Binding of 2-fwmylpyridine monothiosemicarbazone copper ii to cat and normal human hemoglobins. *J. Inorg. Biochem.* 1982;16:145-154.
12. Booth BA, Moore EC, Sartorelli AC. Metabolic effects of some tumor-inhibitory pyridine carboxaldehyde thiosemicarbazones. *Cancer Research.* 1971;31:228-234.
13. Kolessar J, Brundage RC, Pomplun M, Alberti D, Holen K, Traynor A, Ivy P, Wilding G. Population pharmacokinetics of 3-aminopyridine-2-carboxaldehyde thiosemicarbazone (Triapine®) in cancer patients. *Cancer Chemother. Pharmacol.* 2011;67:393-400. DOI: 10.1007/s00280-010-1331-z
14. Iskander MF, El-Sayed L, Zaki KI. Coordination compounds of hydrazine derivatives with transition metals, part 17. nickel (ii) and cobalt(ii) chelates with pyridine-2- aldehyde semi- and thiosemicarbazone. *Transition Met. Chem.* 1979;4:225-230.
15. Kasuga NC, Sekino K, Koumo C, Shimada N, Nomiya K. Synthesis, structural characterization and antimicrobial activities of 4- and 6-coordinate nickel(II) complexes with three thiosemicarbazones and semicarbazone ligands. *J. Inorg. Biochem.* 2001;84:55-65. DOI: S0162-0134(00)00221-X
16. Bamgboye TT, Bamgboye OA. Synthesis and Characterization of Co(II) complexes of 2-pyridinecarboxaldehyde thiosemicarbazone. *Inorg. Chim. Acta* 1985;105:223-226.

17. Chattopadhyay SK, Banerjee T, Roychoudhury P, Mak TCW, Ghosh S. Synthesis, characterization and crystal structure analysis of bis (pyridine-2-carbaldehyde thiosemicarbazonato) cobalt(III) thiocyanate monohydrate. *Transition Met. Chem.* 1999;22:216-219.
18. García-Tojal J, Rojo T. An appraisal of structural, spectroscopic and magnetic aspects of the pyridine-2-carbaldehyde thiosemicarbazonecopper(II) compounds. *Polyhedron.* 1999;18:1123–1130.
19. Kovala-Demertzi D, Miller JR, Kourkoumelis N, Hadjikakou SK, Demertzis MA. Palladium(II) and platinum(II) complexes of pyridine-2-carbaldehyde thiosemicarbazonate with potential biological activity. Synthesis, structure and spectral properties. Extended network via hydrogen bond linkages of [Pd(PyTsc)Cl]. *Polyhedron.* 1999;18: 1005–1013
20. Wang HS, Huang L, Chen ZC, Wang XW, Zhou J, Shi SM, Liang H, Yub KB. Bis(pyridine-2-carbaldehyde thiosemicarbazonato)cobalt(III)perchlorate. *Acta Cryst.* 2004;60:354-356. DOI: 10.1107/S1600536804004763
21. Chandra S, Kumar A. Co(II), Ni(II) and Cu(II) complexes derived from thiosemicarbazonate and semicarbazonate. *Spectrochim. Acta Part A.* 2007;68:1410-1415. DOI: 10.1016/j.saa.2006.12.079
22. Zhou J, Chen ZF, Tan YS, Wang XW, Tan YH, Liang H, Zhang Y. Bis{1-[(E)-2-pyridinylmethylidene]semicarbazide}cobalt (II) diperchlorate monohydrate. *Acta Cryst.* 2004;60:519-521. DOI: 10.1107/S160053680400749
23. Zhou J, Chen ZF, Wang XW, Tan YS, Liang H, Zhang Y. Bis(2-formylpyridine semicarbazonato)nickel(II). *Acta Cryst.* 2004;60:568-570. DOI: 10.1107/S1600536804008207.
24. Garbelini ER, Hörner M, Behm MB, Evans DJ, Nunes FS. Synthesis and crystal structures of bis(1-[(E)-2-pyridinylmethylidene]semicarbazonate) iron(II) and copper(II) diperchlorate monohydrates. *Z. Anorg. Allg. Chem.* 2008;634:1801-1806. DOI: 10.1002/zaac.200800169.
25. Garbelini ER, Hörner M, Giglio VF, da Silva AH, Barison A, Nunes FS. Synthesis, (1-(E)-2-formylpyridine.semicarbazonate) nickel(II) diperchlorate Monohydrate. *Z. Anorg. Allg. Chem.* 2009;635:1236-1241. DOI: 10.1002/zaac.200801358.
26. Garbelini ER, Ribeiro RR, Horner M, Locatelli A, Nunes FS. Preparation, crystallography and spectroscopic properties of the polymeric {(1-(E)-2-pyridinylmethylidene)semicarbazonate}(aqua)copper(II)} sulphate dihydrate complex: Evidence of dynamic Jahn–Teller effect. *Spectrochim. Acta Part A.* 2011;78:1337-1341. DOI: 10.1016/j.saa.2010.12.069.
27. Garbelini ER, Martin MGMB, Back DF, Evans DJ, Santos MM, Ribeiro RR, Lang ES, Nunes FS. Synthesis, characterization and chemical properties of 1-((E)-2-pyridinylmethylidene)semicarbazonate manganese(II) and iron(II) complexes. *J. Mol. Struct.* 2012;1008:35-41. DOI: 10.1016/j.molstruc.2011.11.016
28. Subashchandrabose S, Babu NR, Salem H, Padusa MSA. Vibrational studies on 1-(E)-1-((pyridin-2-yl)methylidene) semicarbazonate using experimental and theoretical method. *J. Mol. Struct.* 2015; 1094:254-263. DOI: 10.1016/j.molstruc.2015.03.062
29. Raman N, Pothiraj K, Baskaran T. DNA interaction, antimicrobial, electrochemical and spectroscopic studies of metal(II) complexes with tridentate heterocyclic Schiff base derived from 2'-methylacetoacetanilide. *J. Mol. Struct.* 2011;1000:135-144. DOI: 10.1016/j.molstruc.2011.06.006.
30. Bembee Devi W, Bhubon Singh RK, Jasinski JP, Golen JA, A new two dimensional copper (II) coordination complex with sulphonamide: Synthesis, crystal structure and DNA binding study. *Inorg. Chem. Comm.* 2012;21:163-167. DOI: 10.1016/j.inoche.2012.05.006
31. Nandy M, Hughes DL, Rosair GM, Bhubon Singh RK, Mitra S. Synthesis, characterization, crystal structure, and DNA binding of two copper(II)–hydrazone complexes. *J. Coord. Chem.* 2014;67: 3335-3353. DOI: 10.1080/00958972.2014.964697
32. Bindiya Devi RK, Pramodini Devi S, Bhubon Singh RK, Hemakumar Singh RK, Swu T, Radhapiyari Devi W, Brajakishore Singh Ch. Synthesis, spectroscopic, and biological studies on copper(II) complexes containing equatorial–apical chloride bridges: crystal structure of [Cu₂(μ-Cl)₂(O-

- 2-butoxyethylpyridine-2-carboximidate) 2Cl₂]. J. Coord. Chem. 2014;67:891-909. DOI: 10.1080/00958972.2014.902449
33. Shantibala Devi N, Jaideva Singh L, Pramodini Devi S, Bhubon Singh RK, Hemakumar Singh RK, Rajeswari B, Kadam RM, Synthesis, spectroscopic and DNA interaction studies on bis(1-amidino-O-2-alkoxyethylurea)Cu(II)nitrate where alkoxy = methoxy, ethoxy or butoxy. J. Mol. Struc. 2014;1076:411-418. DOI: 10.1016/j.molstruc.2014.08.005
 34. Kozlyuk N, Lopez T, Roth P, Acquaye JH. Synthesis and the characterization of Schiff-base copper complexes: Reactivity with DNA, 4-NPP and BNPP. Inorg. Chim. Acta. 2015;428:176-184. DOI: 10.1016/j.ica.2014.12.034.
 35. Guhathakurta B, Basu P, Kumar GS, Lu L, Zhu M, Bandhyopadhyay N, Naskar JP. Synthetic, structural, electrochemical and DNA-binding aspects of a novel oximate bridged copper(II) dimer. Polyhedron. 2016;110:227-234. DOI: 10.1016/j.poly.2016.03.011.
 36. Gupta SK, Sen N, Ganaie JA, Butcher RJ, Jasinski JP. Unusual coordination of mononuclear cobalt(III) complexes with sterically demanding Schiff bases: synthesis, spectroscopy, electrochemistry, crystallography, DNA binding, and theoretical investigation J. Coord. Chem; 2017. DOI: 10.1080/00958972.2017.138019
 37. Alam Md F, Varshney S, Khan MA, Laskar A.A, Younus H. *In vitro* DNA binding studies of therapeutic and prophylactic drug citral. Inter. J. Biol. Macromol; 2018. DOI: 10.1016/j.ijbiomac.2018.02.098
 38. Crys Alis Pro, Agilent Technologies, Version 1.171.36.21, CrisAlis 171.Net; 2012.
 39. Sheldrick GMA. Short history of SHELX. Acta Cryst. 2008;64:112-122. DOI: 10.1107/S0108767307043930.
 40. Dolomanov OV, Bourhis LJ, Gildea RJ, Howard JAK, Puschmann H. OLEX2: a complete structure solution, refinement and analysis program. J. Appl. Cryst. 2009; 42:339-341. DOI: 10.1107/S0021889808042726
 41. Peyronel G, Pellacani GC, Pignedoli A, Benetti G. On the complexes of tetramethyl- and tetraethyl-dithiooxamide with manganese(ii), iron(ii), cobalt(ii), nickel (ii) and copper (ii). Inorg. Chim. Acta. 1971;5:263-269.
 42. Lever ABP. Bidentate nitrate amine metal complexes. Inorg. Chem. 1965;4:1042-1046.
 43. Cotton FA, John J, Wise JJ. Assignment of the electronic absorption spectra of bis(/3-ketoenolate) complexes of copper(ii) and nickel(ii). Inorg. Chem. 1967;6:915-924.
 44. Patel KS, Rinehart KL, Bailar JC. Mass spectral studies of schiff's bases and their metal complexes. Organic Mass Spectrometry. 1970;4:441-451.
 45. Wiecek J, Kovala-Demertzi D, Ciunik Z, Wietrzyk J, Zervou M, Demertzis MA. Organotin compound derived from 3-hydroxy-2-formylpyridine semicarbazone: synthesis, crystal structure, and antiproliferative activity. Bioinorg. Chem. and Appl; 2010. Article ID 718606. DOI :10.1155/2010/718606
 46. Hagen WR. EPR spectroscopy as a probe of metal centres in biological systems. Dalton Trans. 2006;4415-4434. DOI: 10.1039/b608163k
 47. Kivelson D, Neiman R. ESR Studies on the Bonding in Copper Complexes. J. Chem. Phys. 1961;35:149-155. DOI: 10.1063/1.1731880.
 48. Procter IM, Hathaway BJ, Nicholas P. The electronic properties and stereochemistry of the copper(II) ion. Part I. Bis(ethylenediamine)copper(II) complexes. J. Chem. Soc. A: Inorg. Phy. Theo. 1968; 1678-1684. DOI: 10.1039/J19680001678
 49. Reichmann ME, Rice SA, Thomas CA, Doty PA. Further examination of the molecular weight and size of desoxypentose nucleic acid. J. Am. Chem. Soc. 1954;76:3047-3053. DOI: 10.1021/ja01640a067
 50. Marmur JA. Procedure for the isolation of deoxyribonucleic acid from microorganisms. J. Mol. Biol. 1961;3:208-218. DOI: 10.1016/S0022-2836(61)80047-8
 51. Wolfe A, Shimer Jr. GH, Meehan T. Polycyclic aromatic hydrocarbons physically intercalate into duplex regions of denatured DNA. Biochem. 1987;26:6392-6396. DOI: 10.1021/bi00394a013
 52. LePecq JB, Paoletti CA. Fluorescent complex between ethidium bromide and nucleic acids physical-chemical characterization. J. Mol. Biol. 1967;27:87-106. DOI: 10.1016/0022-2836(67)90353-1

53. Liu J, Zhang T, Lu T, Qu L, Zhou H, Zhang Q, Ji L. DNA-binding and cleavage studies of macrocyclic copper(II) complexes. *J. Inorg. Biochem.* 2002;91: 269-276.
DOI: 10.1016/S0162-0134(02)00441-5
54. Lee M, Rhodes AL, Wyatt MD, Forrow S, Hartley JA. GC base sequence recognition by oligo (imidazolecarboxamide) and C-terminus-modified analogues of distamycin deduced from circular dichroism, proton nuclear magnetic resonance, and methidiumpropylethylenediaminetetraacetate-Iron(II) footprinting studies. *Biochem.* 1993;32:4237-4245.
DOI: 10.1021/bi00067a011
55. Lakowicz JR, Weber G. Quenching of fluorescence by oxygen. A probe for structural fluctuations in macromolecules. *Biochem.* 1973;12:4161-4170.
DOI: 10.1021/bi00745a020
56. Li Y, Wu Y, Zhao J, Yang P. DNA-binding and cleavage studies of novel binuclear copper(II) complex with 1,10-dimethyl-2,20-biimidazole ligand. *J. Inorg. Biochem.* 2007;101:283-290.
DOI: 10.1016/j.jinorgbio.2006.10.004
57. Wilson WD, Ratmeyer L, Zhao M, Strekowski L, Boykin D. The search for structure-specific nucleic acid-interactive drugs: effects of compound structure on RNA versus DNA interaction strength. *Biochem.* 1993;32:4098-4104.
DOI: 10.1021/bi00066a035.
58. Baguley BC, Bret ML. Quenching of DNA-ethidium fluorescence by amsacrine and other antitumor agents: A possible electron-transfer effect. *Biochem.* 1984;23: 937-943.
DOI: 10.1021/bi00300a022.
59. Boger DL, Fink BE, Brunette SR, Tse WC, Hedrick MP. A simple, high resolution method for establishing dna binding affinity and sequence selectivity. *J. Am. Chem. Soc.* 2001;123:5878-5891.
DOI: 10.1021/ja010041a
60. Islam GJ, Akhtar HMN, Mamun MA, Ehsan MQ. Investigations on the redox behavior of manganese in manganese(II)-saccharin and manganese(II)-saccharin-1,10-phenanthroline complexes. *J. Saudi Chem. Soc.* 2009;13:177-183.
DOI: 10.1016/j.jscs.2009.05.002
61. Tasa E, Aslanoglua M, Ulusoya M, Temel H. Synthesis, spectral characterization and electrochemical studies of copper(ii) and cobalt(ii) complexes with novel tetradentate salicylaldimines. *J. Coord. Chem.* 2004, 57, 677-684.
DOI: 10.1080/00958970410001720980
62. Kryatov SVB, Mohanraj BS, Tarasov VV, Kryatova, OP, Rybak-Akimova EV, Nickel(II) complexes with tetra- and pentadentate aminopyridine ligands: Synthesis, structure, electrochemistry, and reduction to nickel(i) species. *Inorg. Chem.* 2002;41:923-930.
DOI: 10.1021/ic010397n

© 2019 U-wang et al.; This is an Open Access article distributed under the terms of the Creative Commons Attribution License (<http://creativecommons.org/licenses/by/4.0>), which permits unrestricted use, distribution, and reproduction in any medium, provided the original work is properly cited.

Peer-review history:

The peer review history for this paper can be accessed here:
<http://www.sdiarticle3.com/review-history/48127>